minerals

MDPI

Article

Lithofacies Controls on Hydrocarbon Generation Potentiality of the Syn-Rift Late Cretaceous Rakopi Deltaic Facies in the North-Eastern Offshore Part of Taranaki Basin, New Zealand

Mahmoud Leila [1,*], Ahmed A. Radwan [2] and Mohamed I. Abdel-Fattah [3,4]

[1] Geology Department, Faculty of Science, Mansoura University, Mansoura 11432, Egypt
[2] Department of Geology, Faculty of Science, Al-Azhar University, Assiut Branch, Assiut 71524, Egypt; ahmedabdelhaleim.ast@azhar.edu.eg
[3] Petroleum Geosciences and Remote Sensing Program, Department of Applied Physics and Astronomy, University of Sharjah, Sharjah 27272, United Arab Emirates; mfarag@sharjah.ac.ae
[4] Geology Department, Faculty of Science, Suez Canal University, Ismailia 41522, Egypt
* Correspondence: mahmoud_lotfy@mans.edu.eg

Abstract: The Taranaki Basin in New Zealand presents the most promising territory for strategies of hydrocarbon exploration and development. This basin contains multiple source rock levels in its sedimentary successions formed during syn- and post-rift periods. The deepest source rocks, found in the Rakopi Formation, were deposited in deltaic to deep marine environments and consist of gas-prone coal and organic-rich mudstone lithofacies. However, questions remain about the preservation of their organic carbon. This study integrates various organic geochemical analyses (such as Rock Eval pyrolysis, kerogen petrography, and biomarkers) to assess the hydrocarbon potential of the Rakopi coal and mudstone lithofacies. The organic carbon in Rakopi coals and mudstones originated from oxygenated bottom water, but swift burial during the initial rifting phase facilitated the preservation of organic materials. Rakopi coals are less mature than the mudstone facies and contain a mixture of desmocollinite, suberinite, and resinite macerals. In contrast, the mudstone lithofacies are enriched in liptodetrinite. The maceral mixture in the coal led to its elevated hydrogen index and likely facilitated early expulsion of liquid hydrocarbon phases. Regular steranes, diasteranes, and C29 sterane isomers distribution in the coal and mudstone extracts highlighted a greater terrestrial input in the coals, whereas significant marine input is observed in the mudstone extracts. Biomarkers in the coal and mudstone extracts are similar to some nearby oils discoveries in the Taranaki Basin, thereby confirming oil generation from both coal and mudstone lithofacies in the Rakopi Formation. These findings underscore the potential of liptinite-rich coals to generate liquid hydrocarbon phases at marginal oil maturity levels.

Keywords: Taranaki Basin; source rocks; biomarkers; kerogen; coal; mudstone

Citation: Leila, M.; Radwan, A.A.; Abdel-Fattah, M.I. Lithofacies Controls on Hydrocarbon Generation Potentiality of the Syn-Rift Late Cretaceous Rakopi Deltaic Facies in the North-Eastern Offshore Part of Taranaki Basin, New Zealand. *Minerals* **2023**, *13*, 1169. https://doi.org/10.3390/min13091169

Academic Editor: Thomas Gentzis

Received: 23 July 2023
Revised: 28 August 2023
Accepted: 31 August 2023
Published: 3 September 2023

1. Introduction

The content of total organic carbon "TOC" and the quality and maturity of the organic matter are the main factors controlling the hydrocarbon generation capability of the source rock [1–5]. In addition, the depositional environment and the provenance of the source rock sediment influence both the primary productivity and preservation of the organic matter [6–8]. Furthermore, the lithology of the source rock controls the maturation pathway of the source rock and hence the expulsion timing and conditions [9–12]. For example, mudstone source rocks enriched in vitrinite-rich kerogen exhibit an early release of liquid hydrocarbons upon reaching the oil window maturity stage. However, hydrocarbon retention in the tiny pore spaces of the mudstones hinders the full expulsion phase of the liquid hydrocarbons. Moreover, liptinite-rich source rocks require prolonged exposure to pressure and temperature prior to the expulsion of liquid hydrocarbon phases [12]. Thus,

a detailed investigation of the primary source rock characteristics (e.g., organic matter quantity and maturity) as well as identification of the kerogen composition are crucial for understanding the generation and expulsion potentiality of the source rock.

The Taranaki Basin is the most petroliferous and the only hydrocarbon-producing sedimentary basin in New Zealand, where the majority of petroleum reserves are contained in a broadly NE-SW trending fairway of the Paleogene shallow marine as well as Pliocene turbiditic sandstones (Figure 1) [13–21]. Based on previous geochemical studies, it has been revealed that oils are primarily sourced from the terrigenous organo-facies in the Late Cretaceous-Paleocene source rocks that rest unconformably above the basement complex. Most of these studies have been focused on the Late Cretaceous Pakawau Group of Rakopi and North Cape Formations [22–32]. Globally, the Late Cretaceous sedimentary successions host potential source rock organo-facies deposited during the oceanic anoxic events, which allowed optimum preservation for organic materials [33–35]. In the Taranaki Basin, the Upper Cretaceous sediments of the Rakopi Formation were accumulated in a fluvio-marine depositional environment, thus hosting variable lithofacies with different kerogen compositions (Figure 2). However, the link between lithofacies type, kerogen composition, and source rock generation potential, as well as the type of the generated hydrocarbon phases, requires further investigation. Therefore, in order to decipher this link, we investigate the kerogen composition and geochemical characteristics of different lithofacies (coal and mudstone) from Rakopi deltaic facies and correlate them with bitumen extracts.

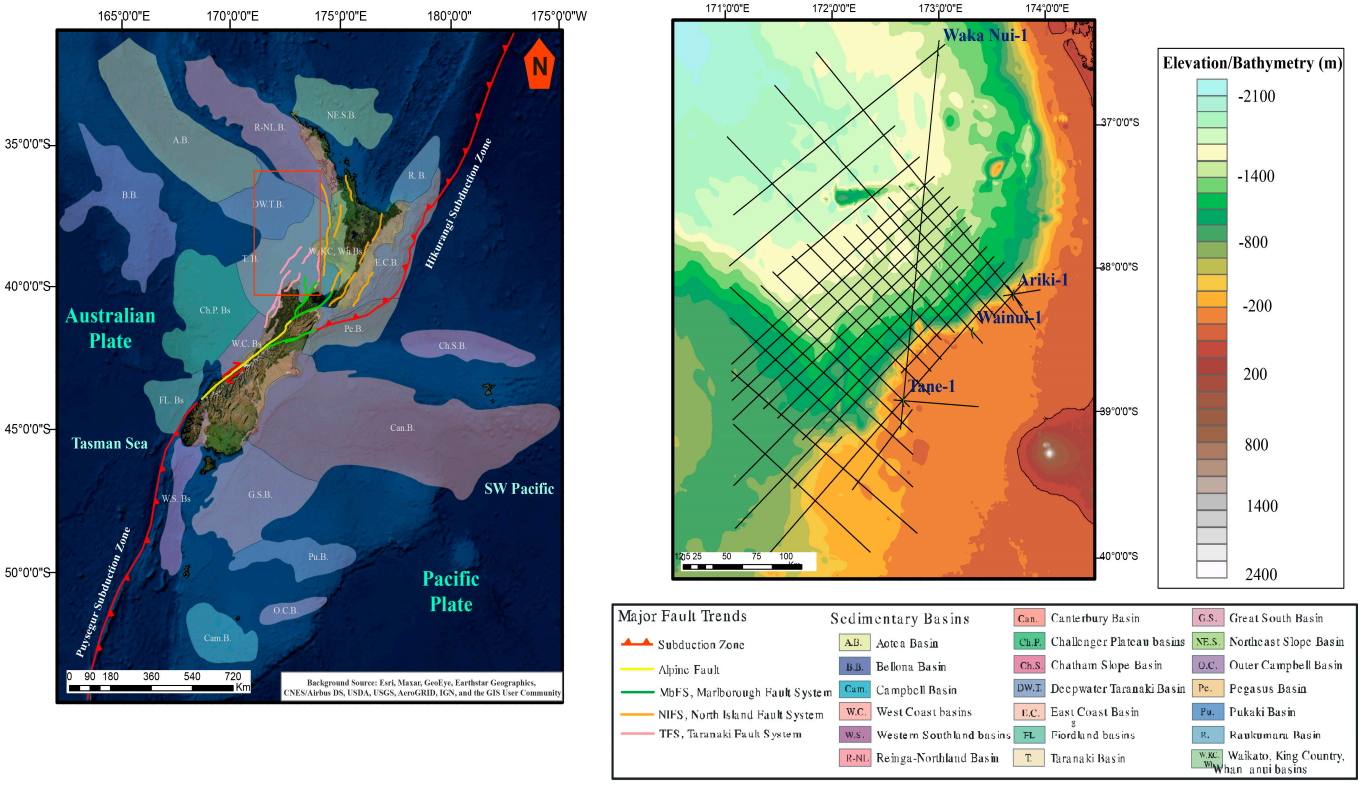

Figure 1. A map illustrates the area of study in the northeastern offshore part of the Taranaki Basin, New Zealand. The map on the right, which illustrates the studied wells, presents an enlarged view of the red rectangle on the left map [19].

2. Geologic Setting

The evolution of the Taranaki Basin coincides with late Cretaceous syn-rift extensional faulting related to the break-up of eastern Gondwana coupled with the formation of fault-bounded graben and half-graben structures (Figure 3) [15,16,36–43]. The Taranaki Basin constitutes two main structural provinces: the Eastern Mobile Belt (Taranaki Graben) and

the Western Stable Platform. The Eastern Mobile Belt, which includes the study region, is dominated by several grabens and contains a variety of compressional features such as overthrusts, reverse faults, and inversion structures (Figure 1); the Western Platform is a comparatively undeformed and stable block. Extension and subsidence along the rift faults caused the accumulation of shallow to deep marine facies in the structural lows. Cyclic variation in fault offsets caused lateral and vertical facies variability across the basin. The syn-rift facies contain a progression from non-marine conglomerates to sand, silt, and coals of the Rakopi and North Cape Formations (Figure 2) [15,36]. By the Early Eocene, the Taranaki Basin changed into a passive margin with a drift and regional subsidence leading to marine transgression with widespread deposition of terrestrial to marginal marine sediments of the "Kapuni Group", which comprises Farewell, Kaimiro, Mangahewa, and McKee Formations (Figure 2) [15,16,44].

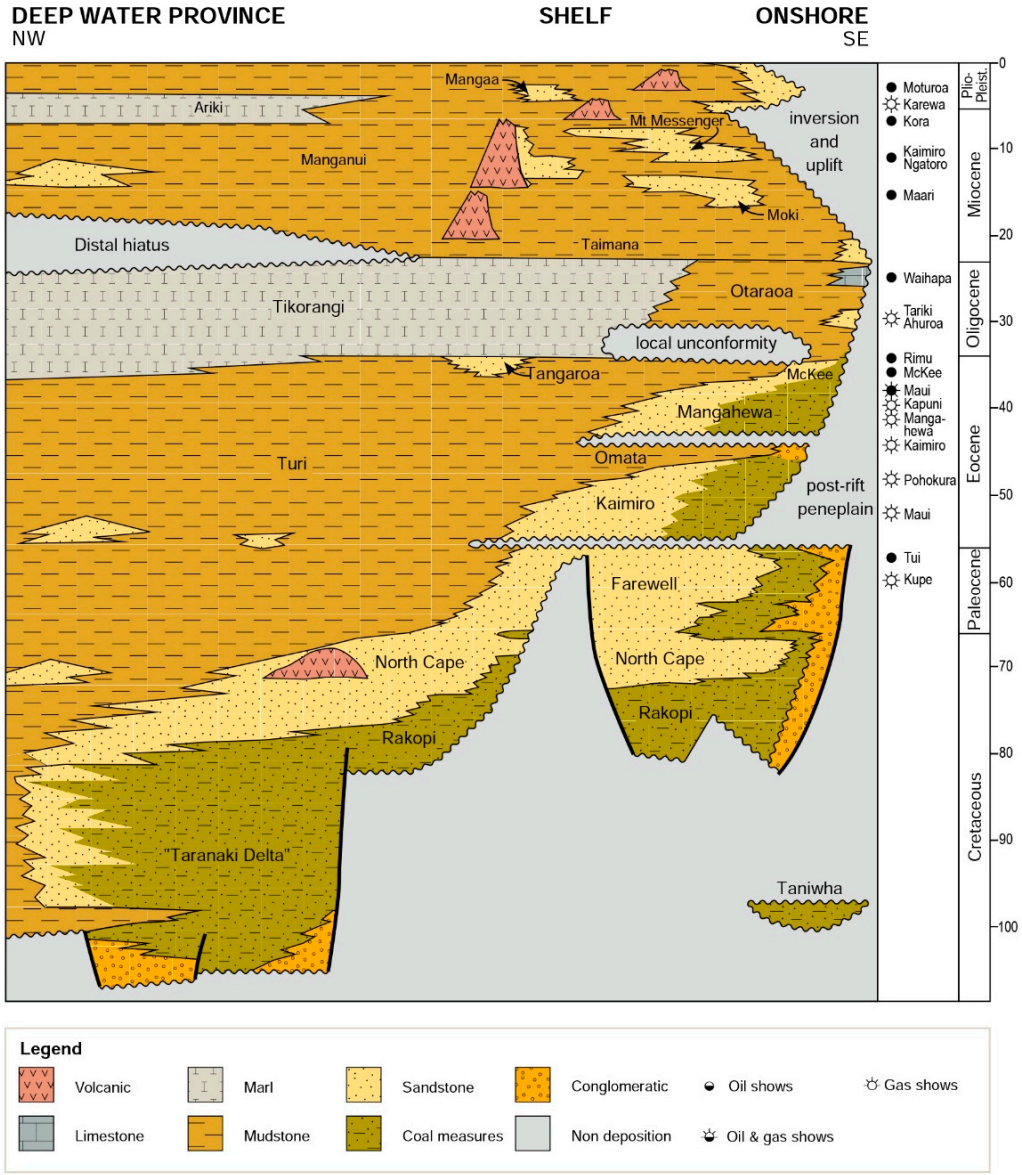

Figure 2. Generalized lithostratigraphic column along the different territories of the Taranaki Basin demonstrates the main tectono-stratigraphic units (compiled from [15,45–47]).

Compressional tectonics prevailed during the Late Eocene, thereby reactivating the rift faults to coincide coupled with an increased uplift rates along the Alpine Fault on the South Island of New Zealand, which has also been linked to the nearby subduction zone that affected the Upper Eocene successions. Oligocene tectonic quiescence and compression in response to a developing Hikurangi subduction zone coupled with a decline in clastic supply resulted in extensive deposition of limestone (Tikorangi Formation) and calcareous mudstone (Otaraoa Formation). This transgressive phase peaked in the Early Miocene during the deposition of the Ngatoro Group: Taimana formation and Wai-iti Group: Manganui formation. During the Miocene—recent times—the basin transformed into an active marginal region attributed to a change in stress regime in response to the development of the Australia-Pacific convergent plate boundary of the Hikurangi Subduction System through New Zealand [15].

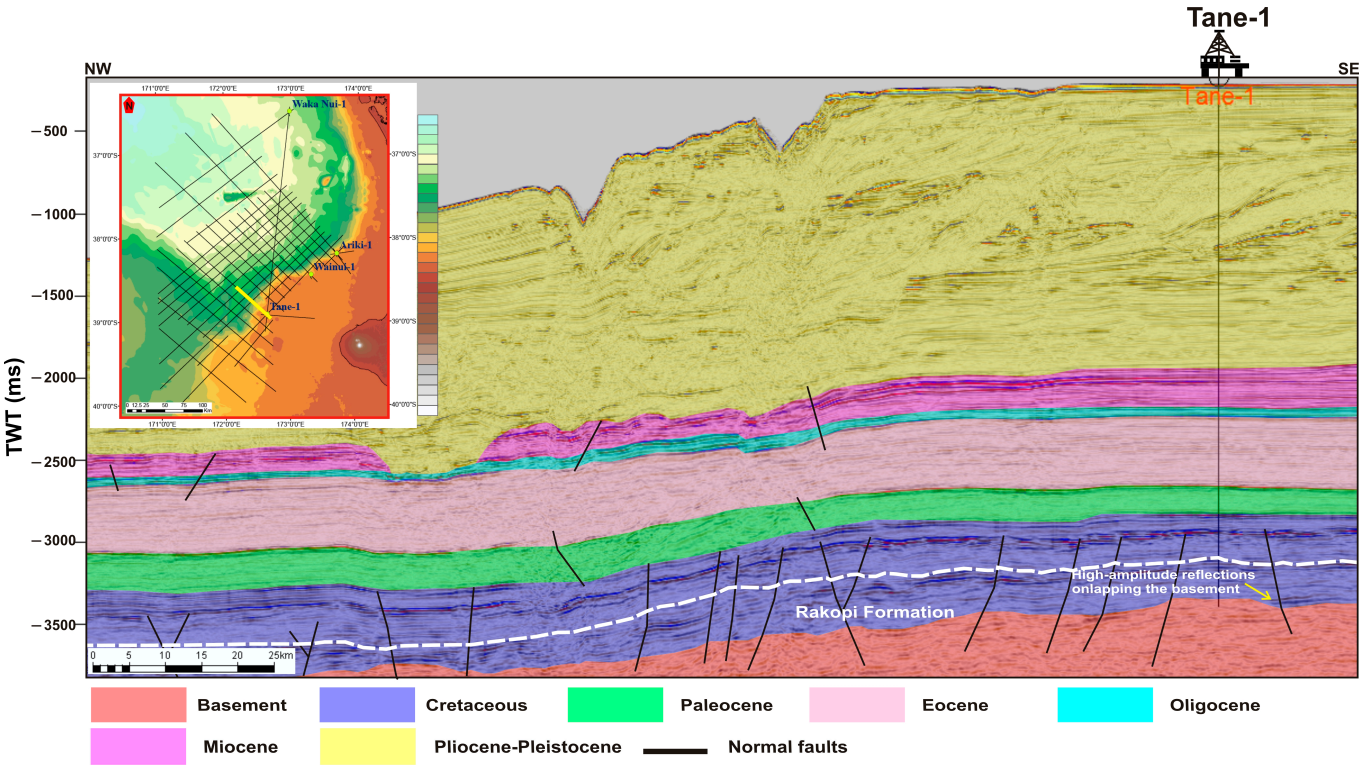

Figure 3. Interpreted 2D seismic profile demonstrating the main structural trends in the study region. The profile illustrates the accumulation of Upper Cretaceous syn-rift facies unconformably above the basement complex.

3. Data and Methods

3.1. Total Organic Carbon "TOC" and Rock-Eval Pyrolysis Analysis

This analysis was conducted on 13 cutting and side wall core (SWC) samples retrieved from three wells (Tane-1, Wainui-1, and Waka Nui-1; Figure 1) in the offshore north-western part of the Taranaki Basin. TOC and Rock-Eval pyrolysis measurements were performed by Applied Petroleum Technology (APT), Norway. For this, the samples were firstly crushed and washed with distilled water and dichloromethane solvent for the removal of hydrocarbon residues. A Leco CS-632 high-temperature combustion oven (Leco inc Company, St. Joseph, MI, USA) was utilized for the measurement of total organic carbon (TOC). High-temperature (~1300 °C) oxidation of the samples was performed, and the oxidized organic carbon was measured using a solid-state infrared detector. Rock-Eval-6 apparatus (built by Vinci technologies, Bedfordshire, UK) was utilized to measure the Rock-Eval pyrolysis parameters (S1, S2, and S3) following the procedure of [48]. The TOC and Rock-Eval pyrolysis parameters were then used to deduce several important source rock quality pa-

rameters such as hydrogen and oxygen indices (HI = Rock Eval S2/TOC × 100; OI = Rock Eval S3/TOC) × 100, respectively), and production index (S1/(S1 + S2). These parameters reflect the capability of the studied samples to generate hydrocarbon phases [1–3].

3.2. Total Sulfur "TS" Analysis

The content of total sulfur "TS" in the studied 13 cutting and SWC samples was measured using a Leco analyzer (Leco inc Company, St. Joseph, MI, USA). The analysis was performed on the powdered samples at the Applied Petroleum Technology (APT) institute, Norway. This analysis involves a high-temperature (~1800 °C) combustion of approximately 20 mg of dry, powdered sample in the presence of oxygen. An infrared detector is used to detect the released SO_2 gas during the oxidation, directly inferring the total sulfur content within the sample which mostly constitutes sulfate sulfur, iron sulfur, as well as organic sulfur [49].

3.3. Vitrinite Reflectance and Kerogen Petrography

Analyses of organic petrography were carried out at the Applied Petroleum Technology (APT) Institute, Norway, on 11 cutting and SWC samples. The reflectivity of vitrinite particles (%Ro) was measured by a Zeiss MPM 03 Photometer (Zeiss group, Oberkochen, Germany). Prior to petrographic analysis, the samples were crushed and sieved using a 63 µm sieve and then embedded in epoxy resin to prepare polished thin sections. The latter were examined under incident white and UV light under oil immersion. The reflectivity measurements were reported using a 546 nm wavelength monochromatic light [3,50]. The polished thin sections were also examined using an Axioplan 2 imaging Zeiss microscope (Zeiss group, Oberkochen, Germany) in order to assess the main components of the kerogen as exinite, liptinite, and inertinite.

3.4. Biomarker Analysis

Biomarker analyses were conducted on thirteen rock extract samples from the studied Tane-1, Wainui-1, and Waka Nui-1 wells. Bitumen was extracted from the powdered cutting and SWC samples using a Dionex Accelerated Solvent Extraction unit (ASE 350) (Thermo Fisher scientific, Waltham, MA, USA). Approximately 4 to 5 g of powdered sample were mixed with 1–2 g of a dispersant (acid-washed sand). The samples were packed into 11 mL stainless steel Dionex ASE cells on top of a 21 mm Whatman Glass microfiber filter inserted into the base cap and a small 2–3 mm plug of acid-washed sand. The sample was tapped firmly on the bench to ensure adequate compaction in order to extract as much material as possible. A small layer of acid-washed sand was placed over the sample before the lid was screwed on. The prepared cell was loaded into the ASE 350 upper carousel, and two 100 mL collection bottles were loaded into the lower carousel for the collection of the extract. The cell was extracted using a 95:5 vol/vol dichloromethane/methanol (DCM:MeOH) mix at 100 °C (heating time 5 min) at 1000 psi for 2 min static time using a 120% flush for 5 cycles. A 300-second nitrogen purge was used to displace the solvent. The entire procedure was repeated in the second collection bottle to ensure the sample was completely extracted. After extraction, the DCM:MeOH mix was removed using a rotary evaporator.

Bitumens from ASE-extracted source rocks were separated into various fractions before analysis (saturates, aromatics, and asphaltenes). Asphaltenes were precipitated by adding at least 40 times the extract volume of n-hexane. The saturate fraction was separated using a silica + activated alumina column [51]. Prior to elution, the Si + Al column was conditioned with n-hexane. The sample was then introduced onto the column and eluted with n-hexane.

Carbon isotope composition of the separated fractions was carried out using a Micromass IsoPrime instrument (IsoPrime Ltd, Cheadle Hulme, UK) interfaced with a HP6890 gas chromatograph (GC) equipped with a HP7683 autosampler operated in split/splitless mode and fitted with a 60 m × 0.25 mm i.d. DB-5 column (0.25 µm film thickness). The oven of the apparatus was programmed from 40 °C to 300 °C at 8 °C/min. The carrier

gas (helium) was adjusted at a flow rate of 1.5 mL/min using a constant flow injector. The separated samples were dissolved in n-hexane. The carbon isotope ratios were measured relative to CO_2 pulses utilizing CO_2 gases of known $\delta^{13}C$ contents in the mass spectrometer. The values of stable carbon isotopes were presented in the delta notation (δ) relative to the known carbonate standard (Vienna Pee Dee Belemnite VPDB). $\delta^{13}C$ values are generally averaged from at least three sample runs and accepted results typically have a standard deviation of <0.5‰.

The analysis of gas chromatography–mass spectrometry (GC-MS) was carried out on the saturate fraction using A Hewlett-Packard (HP) 5975C MSD interfaced (Hewlett-Packard, Palo Alto, CA, USA) to a HP7890A gas chromatogram fitted with a 25 m × 0.25 mm a fused silica capillary column. The carrier helium gas was flowed at a linear velocity of 1 mL/min using the constant flow injector. The GC oven was ramped from 40 °C to 300 °C at a heating rate of 5 °C/min with initial and final hold times of 3 and 20 min, respectively. Using a Combi-Pal auto-sampler, 2 µL injections in n-pentane or n-hexane with a 10:1 split were made on-column. The mass spectrometer was operated with an ionization energy of 70 eV, a temperature of 230 °C, and equipped with an electron multiplier voltage of 1424 V and a range of scanning mass between 50 and 550 atomic mass unit (amu). The different GC-MS ions aid in the identification of different biomarker components; ions 191 and 217 were used to identify the terpenes and steranes components which aid in the interpretation of depositional environment and maturity of the studied extracts and hence allow the oil–source rock correlation.

4. Results and Interpretation

4.1. Total Sulfur "TS" and Total Organic Carbon "TOC" Contents

The studied Rakopi coal facies display a wide range of total sulfur content in the range of 0.67–3.1 wt% with an average content of 1.35 wt% (Table 1). The coal samples also display a very high TOC content (43–72 wt%) with an average TOC of 62 wt%. On the other hand, the Rakopi mudstones display comparatively lower TS and TOC contents with average values of 0.70 wt% and 20 wt%, respectively. The TOC versus TS plot provides insights on the depositional conditions of the source rocks. A relative enrichment of sulfur indicates deposition in anoxic to euxinic conditions, whereas the depletion of sulfur relative to TOC would infer oxygenated environment [52,53]. Accordingly, most of the studied coal and mudstone facies were deposited in oxic to suboxic conditions (Figure 4). Elevated TOC contents in the studied lithofacies despite their deposition in well-oxygenated conditions suggest a rapid burial of the organic matter in their sediments which prompted its preservation [54]. This rapid burial was likely accompanied by increased primary productivity coupled with high influx of terrigenous and carbonaceous materials.

Table 1. Total sulfur "TS", total organic carbon "TOC", Rock-Eval pyrolysis, and vitrinite reflectance results for the studied coal and mudstone facies.

Well	Lithology	TS Wt (%)	TOC Wt (%)	S_2 Mg HC/g Rock	HI Mg HC/g TOC	VR (%Ro)
Tane-1	Coal	1.67	69.53	200.95	289	0.51
Tane-1	Coal	0.67	71.85	198.30	276	0.66
Tane-1	Coal	0.65	71.67	169.85	237	0.68
Tane-1	Coal	0.67	71.14	177.85	250	0.76
Wainui-1	Coal	-	43.2	-	-	0.49
Wainui-1	Coal	-	44.0	-	-	0.45
Wainui-1	Coal	3.07	60.26	227.18	377	0.48
Average		1.35	62	195	286	0.57

Table 1. *Cont.*

Well	Lithology	TS Wt (%)	TOC Wt (%)	S_2 Mg HC/g Rock	HI Mg HC/g TOC	VR (%Ro)
Tane-1	Mudstone	0.76	33.63	102.57	305	0.66
Tane-1	Mudstone	0.65	38.48	102.74	267	0.71
Tane-1	Mudstone	0.66	39.04	105.79	271	0.76
Wainui-1	Mudstone	-	28.55	107.34	376	0.48
Wainui-1	Mudstone	-	5.0	-	-	0.54
Wainui-1	Mudstone	-	0.78	2.51	322	0.97
Wainui-1	Mudstone	-	9.31	15.6	168	1.03
Wainui-1	Mudstone	-	5.50	7.18	131	1.06
Average		0.70	20	63.4	263	0.78

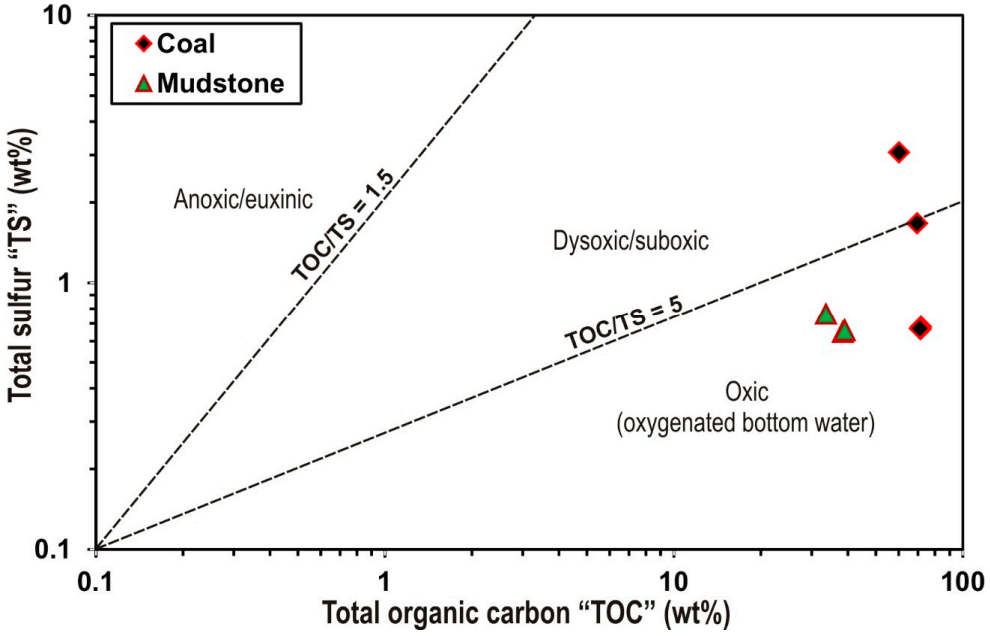

Figure 4. Total organic carbon "TOC" versus total sulfur "TS" plot illustrates the paleoredox depositional conditions of the studied Rakopi coal and mudstone facies.

4.2. Rock-Eval Pyrolysis

The Rock-Eval pyrolysis parameters differ greatly in the studied Rakopi coal and mudstone facies. Rock-Eval S2 values are much higher in the coal than in the mudstone facies. S2 values range in the coal facies from 170 to 227 mg HC/g rock with an average of 195 mg HC/g rock, whereas the maximum S2 value in the mudstones is 107 mg HC/g rock with an average of 63.4 mg HC/g rock (Table 1). The TOC versus Rock-Eval S2 plot demonstrates that the mudstone samples are classified as fair to excellent source rocks, whereas the coal samples have an excellent ability to generate hydrocarbon up to reaching the hydrocarbon generation window maturity (Figure 5A). The Rock-Eval S2 and TOC values in the studied facies reveal that the majority of the studied coal and mudstone are enriched in type III kerogen; however, a few samples with significant type II kerogen materials also exist (Figure 5B).

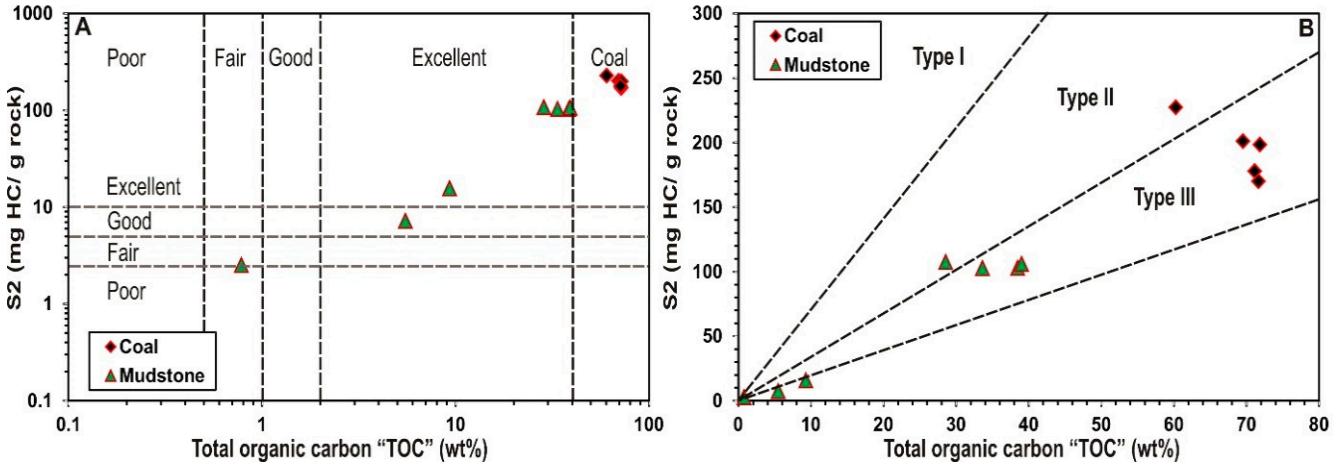

Figure 5. Total organic carbon "TOC" versus Rock-Eval S2 plots demonstrate the excellent source rock characteristics of the studied facies (**A**) which are mostly classified as type III kerogen (**B**).

The calculated hydrogen index (HI) values are high in all the studied samples, with an average values of 286 mg HC/g TOC and 263 mg HC/g TOC in the coal and mudstone facies, respectively (Table 1). The TOC versus HI plot typifies that most of the studied samples are potential gas source rocks; however, the ability of some mudstone samples to generate both oil and gas is ruled out (Figure 6A). Notably, the measured vitrinite reflectance values are greater in the mudstone than in the coal facies. The majority of coal samples are immature (Figure 6B), with vitrinite reflectance values ranging from 0.48 %Ro and 0.76 %Ro (Table 1). Therefore, the coal samples can generate either biogenic gases or mature liquid hydrocarbon phases. In contrast, the mudstone facies are principally in the oil window maturity level (average = 0.78 $\%R_0$), except only two samples with reflectance values < 0.6 $\%R_0$.

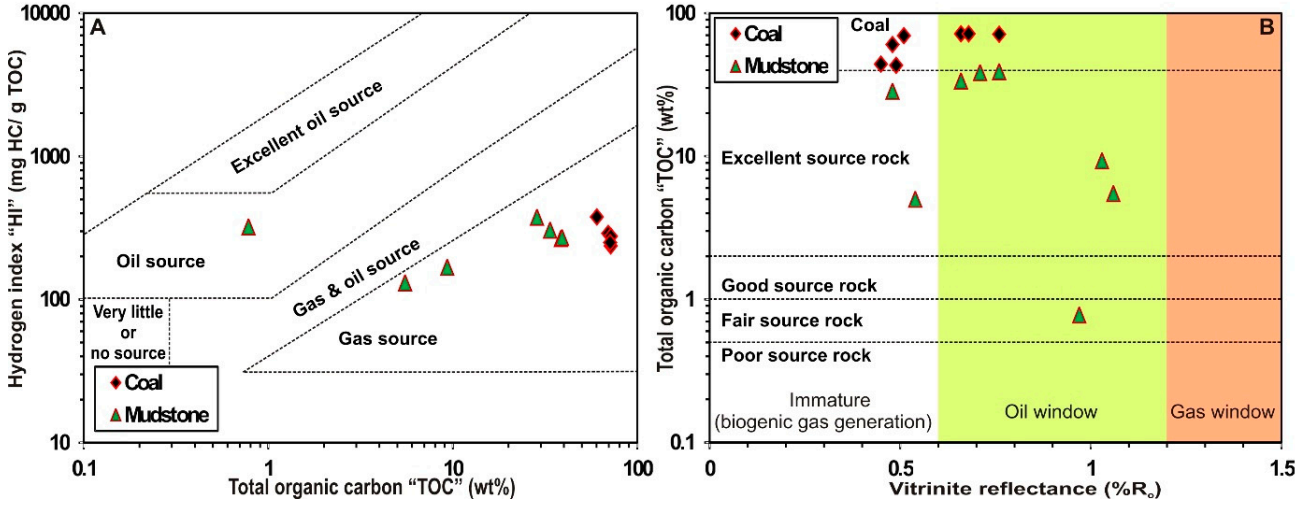

Figure 6. Total organic carbon "TOC" versus HI plot typifies that the coal and mudstone facies are classified as gas sources (**A**); vitrinite reflectance versus TOC plot illustrates the immaturity to oil-window maturity level of the studied facies (**B**).

4.3. Organic Petrography

Rakopi coal facies consist mainly of vitrinite which occurs in the form of desmocollinite, while other vitrinite phases are completely absent (Figure 7A–C). Notably, all the coal samples contain subordinate contents of liptinite maceral. The latter occurs in the form of resinite (Figure 7A), cutinite, and liptodetrinite (Figure 7B,C). Sapropelic organic matter occurs in some samples (Figure 7C), typifying a mixed input from marine organisms.

Similar to coals, the mudstone facies are enriched in desmocollinite; however the liptinite maceral is more abundant (Figure 7D–F). Liptinite occurs mostly in the form of banded cutinite, desmocollinite, as well as cellular suberinite. Notable, inertinite occurs as traces of fusinite (Figure 7D). Pyrite occurs in trace amounts in all the studied samples (Figure 7A).

The relative contents of vitrinite, liptinite, and inertinte demonstrate the kerogen type as well as the type of hydrocarbon generated from the source rocks [53–56]. Most of the studied coals have vitrinite contents exceeding 85%, thus classified as gas-prone source rocks (Figure 8). On the other hand, all the mudstone samples contain subordinate contents of liptinite, and are therefore capable of producing principally gas; however, their potentiality to generate liquid phases cannot be excluded.

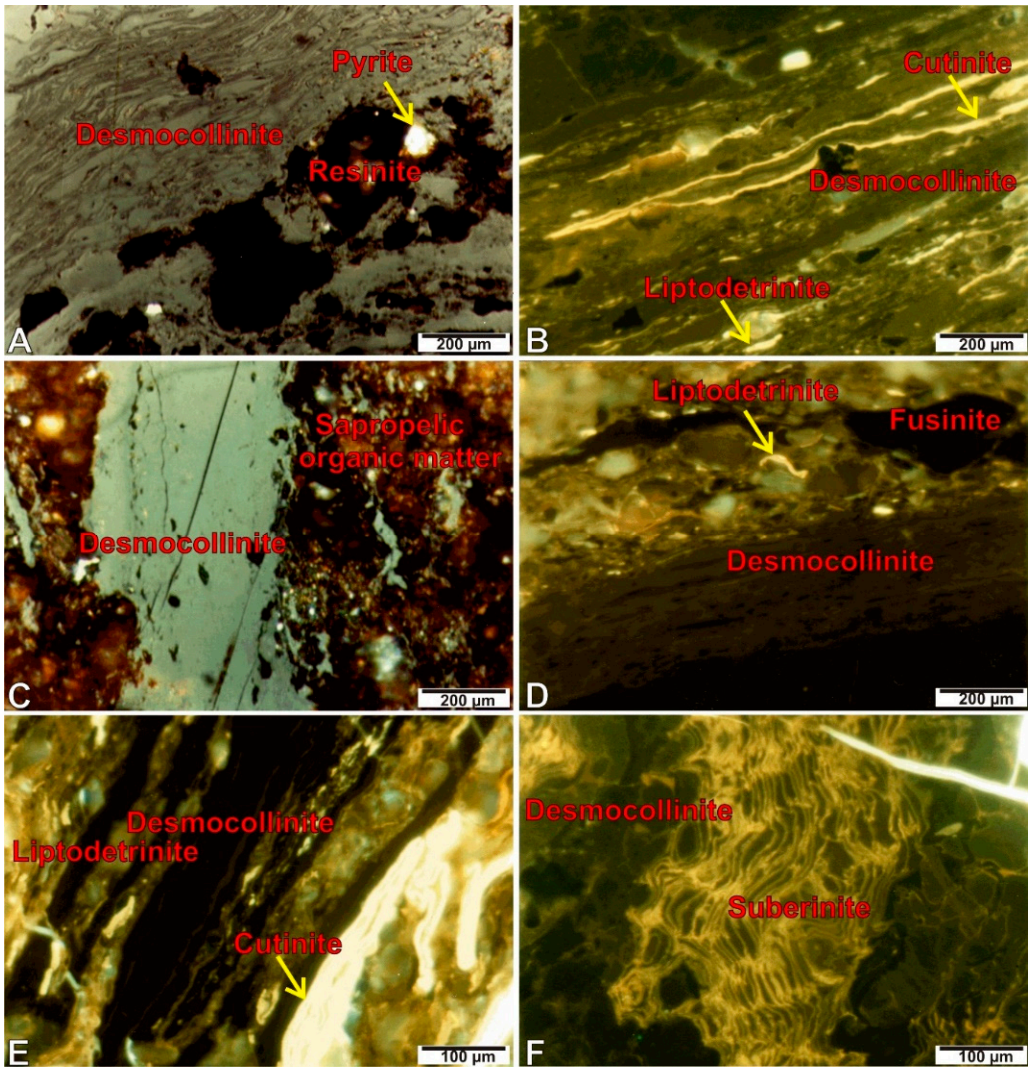

Figure 7. Microphotographs illustrates the maceral composition of the coal (**A**–**C**) and mudstone facies (**D**–**F**). Yellow arrows refer to the maceral and mineralogical components.

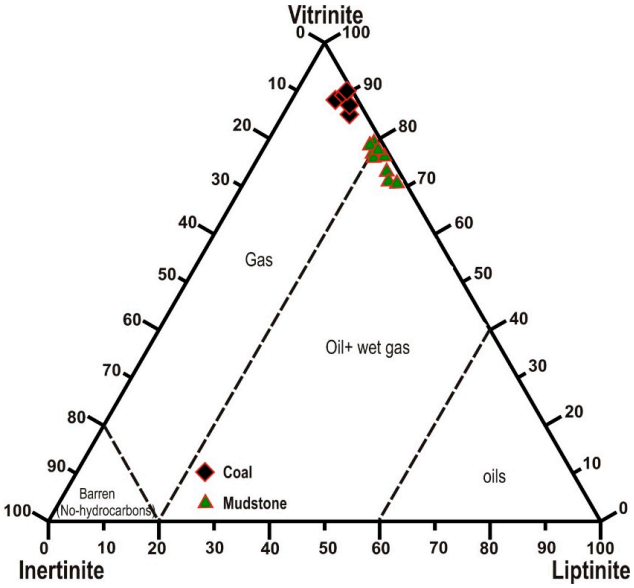

Figure 8. Vitrinite-liptinite-inertinite ternary plot of the studied coal and mudstone facies. Interpretation fields are based on [53].

4.4. Biomarker Analysis

4.4.1. Bulk Composition and n-Alkane Distribution

The bulk composition of the coal and mudstone extracts is dominated by asphaltene and polar compounds relative to both saturate and aromatic hydrocarbons. The coal extracts display an average composition of 4.8 wt%, 25 wt%, and 70.2 wt% for saturates, aromatics, and asphaltene + polar compounds, respectively. On the other hand, the mudstones are more enriched in saturates relative to aromatics, thereby displaying an average composition of 18.7 wt%, 14 wt%, and 67.3 wt%, respectively (Table 2). Such depletion of saturated hydrocarbons is most likely due to their preferential removal either by bacterial biodegradation or water washing (e.g., [57,58]). The extract samples display a narrow range of $\delta^{13}C_{saturates}$ and $\delta^{13}C_{aromatics}$ with average values of −28.42‰, −26.81‰, and −28.17‰, −26.90‰ in the coal and mudstone extracts, respectively (Table 2). The canonical variable values are greater in the coal than that in the mudstone extract samples (Table 2).

Table 2. Bulk compositional characteristics and normal alkane distribution results of the studied coal and mudstone extracts.

Well	Lithology	Saturates Wt (%)	Aromatics Wt (%)	Asphaltene & Polar Compounds Wt (%)	$\delta^{13}C_{saturates}$ (‰)	$\delta^{13}C_{aromatics}$ (‰)	Canonical Variable CV	Pr/Ph	Pr/nC_{17}	Ph/nC_{18}	CPI
Tane-1	Coal	3.4	26.7	69.9	−29.0	−26.6	2.67	5.69	7.88	1.14	1.59
Tane-1	Coal	5.7	24.4	70.0	−28.5	−26.9	0.74	8.83	8.78	0.87	1.55
Tane-1	Coal	5.6	18.3	76.1	−28.5	−27.3	−0.15	8.12	7.38	0.86	1.57
Tane-1	Coal	5.2	13.9	81.0	−29.1	−26.5	3.14	5.03	3.76	0.96	1.55
Tane-1	Coal	5.4	28.6	65.9	−27.5	−26.5	−0.91	8.16	3.22	0.36	1.29
Tane-1	Coal	3.6	31.8	64.7	−28.1	−27.1	−0.72	7.16	2.86	0.37	1.25
Wainui-1	Coal	5.2	31.8	63.1	−28.3	−26.8	0.45	8.30	8.30	1.10	1.38
Average		4.8	25.0	70.2	−28.42	−26.81	0.74	7.32	6.02	0.80	1.45
Wainui-1	Mudstone	11.0	19.9	69.1	−28.3	−26.8	0.45	4.42	2.09	0.44	1.35
Wainui-1	Mudstone	15.3	9.0	75.6	−28.1	−26.9	−0.28	3.73	1.65	0.43	1.36
Wainui-1	Mudstone	29.9	13.3	56.7	−28.1	−27.0	−0.50	4.22	1.96	0.50	1.36
Wainui-1	Mudstone	-	-	-	–	–	–	3.50	2.30	0.58	1.17
Average		18.7	14.0	67.3	−28.17	−26.90	−0.11	3.97	2.00	0.49	1.31

The coal and mudstone extracts display bimodal n-alkane distribution with a relative abundance of heavy molecular weight alkanes (Figure 9). The studied extracts have elevated pristane/phytane (pr/ph) ratios > 3.5 (Table 2), and they are enriched in pristane relative to other isoprenoids and n-alkanes, thereby displaying pr/nC17 > 1.5. On the other hand, most of the samples are depleted in phytane and display ph/nC18 values < 1. The carbon preference index (CPI) is greater than 1 in all the studied extracts, with average CPI values of 1.45 and 1.1 in the coal and mudstone extracts, respectively.

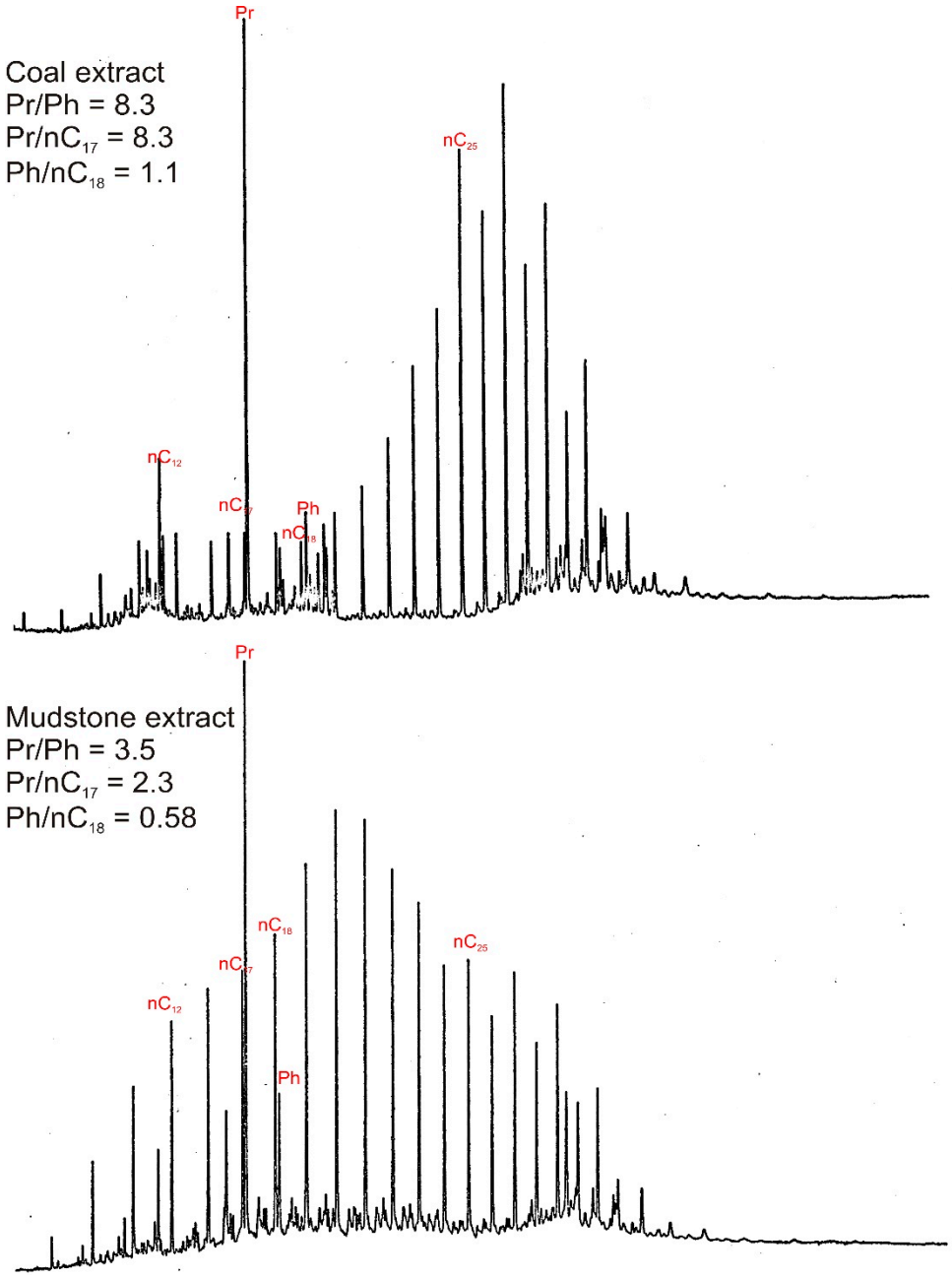

Figure 9. Selected gas chromatograms show the n-alkane distribution in the studied coal and mudstone extracts.

4.4.2. Terpanes and Steranes

The studied extracts are enriched in C_{29} and C_{30} hopanes relative to tricyclic and tetracyclic terpenes (Figure 10A). The extracts are depleted in diterpanes and gammacerane relative to C_{30} hopane. The coal and mudstone extracts display a similar gammacerane index with average values of 0.28 (Table 3). Oleanane occurs in elevated concentrations in

most of the studied extracts suggesting a significant contribution from terrestrial higher plants [59,60]. The mudstone extracts higher trisnorhopanes ratio (Ts/(Ts + Tm) than the coal extracts, where values greater than 0.1 are only observed in the mudstone extracts. The extracts are all depleted on diahopanes relative to hopanes with average values of 0.06 and 0.08 for the coal and mudstone extracts, respectively. Additionally, the mudstone extracts are more enriched in C_{23} tricyclic terpane and display an average C_{23} tricyclic terpane/(C_{23} tricyclic terpane + C_{30} hopane) value of 0.39, whereas the coal extracts are relatively depleted in C_{23} tricyclic terpane with average C_{23} tricyclic terpane/(C_{23} tricyclic terpane + C_{30} hopane) of 0.09. On the other hand, the coal extracts are enriched in C_{19} tricyclic terpanes relative to C_{23} tricyclic with average C_{19} tricyclic terpane/(C_{19} tricyclic terpane + C_{23} tricyclic) value of 0.77. In contrast, the mudstone extracts are depleted in C_{19} tricyclic terpanes and display an average C_{19} tricyclic terpane/(C_{19} tricyclic terpane + C_{23} tricyclic) of 0.36. Such variation in some specific tricyclic terpanes components in the coal and mudstone extracts typify a slight variation in the kerogen composition (e.g., [4,57]).

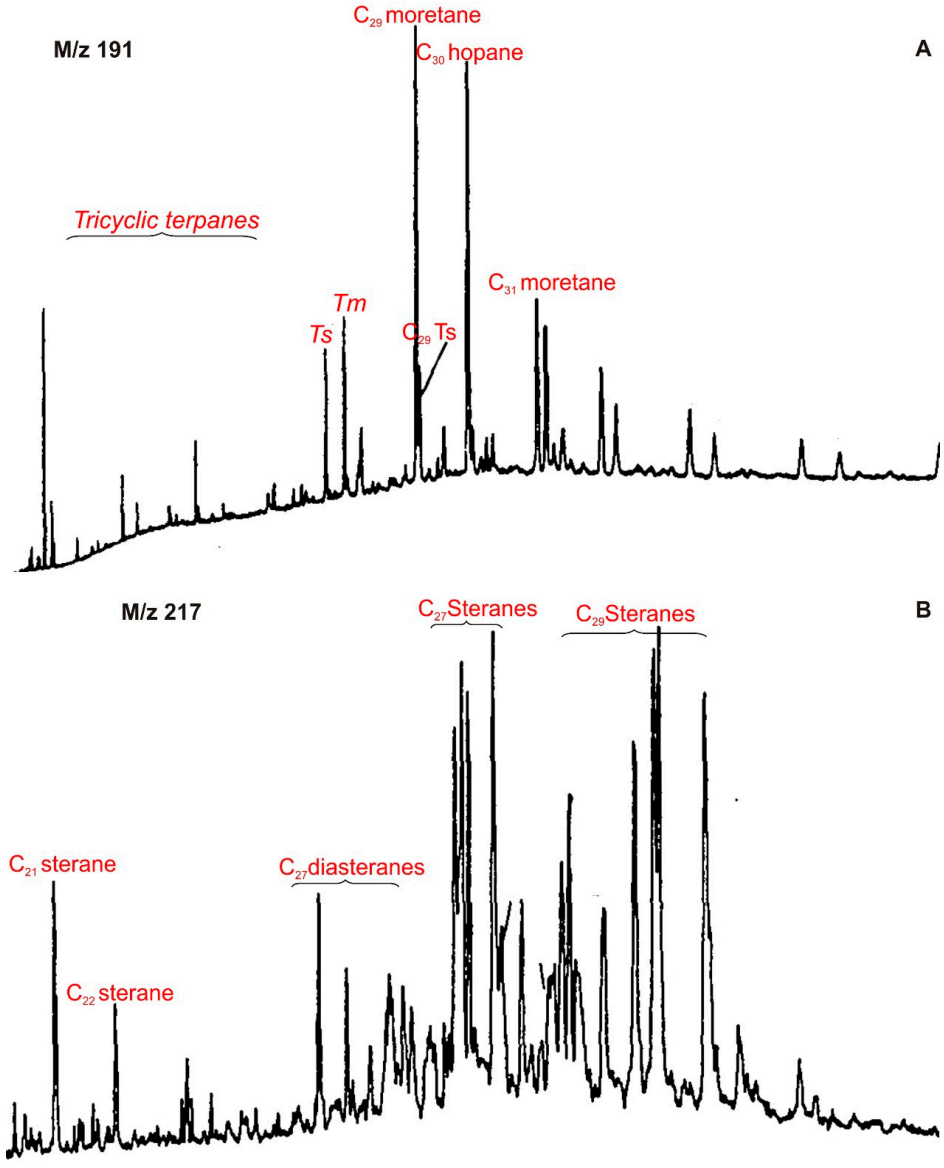

Figure 10. Selected GC/MS ion fragmentograms illustrate the terpanes (**A**) and steranes (**B**) distribution in the studied extracts.

Table 3. Distribution results of some selected terpanes and steranes in the studied coal and mudstone extracts.

Well	Lithology	A	B	C	D	E	F	G	H	I	J	K	L	M
Tane-1	Coal	0.03	3.45	0.36	0.06	0.12	0.74	4.76	10.18	19.09	70.74	0.44	0.46	0.39
Tane-1	Coal	0.02	3.74	0.20	0.04	0.05	0.85	4.82	5.30	11.67	83.03	0.34	0.49	0.35
Tane-1	Coal	0.03	9.60	0.23	0.06	0.09	0.74	7.08	6.77	12.33	80.90	0.38	0.48	0.31
Tane-1	Coal	0.08	18.89	0.30	0.09	0.17	0.67	10.41	13.41	13.42	73.17	0.50	0.47	0.40
Tane-1	Coal	0.02	-	0.19	0.03	0.03	0.90	3.39	5.07	13.80	81.13	0.19	0.52	0.40
Tane-1	Coal	0.12	5.57	0.43	0.05	0.06	0.82	5.31	9.14	29.44	61.42	0.26	0.46	0.39
Wainui-1	Coal	0.09	11.64	0.26	0.12	0.13	0.70	10.20	9.42	13.53	77.05	0.31	0.47	0.40
Average		0.06	7.55	0.28	0.06	0.09	0.77	6.57	8.47	16.18	75.35	0.34	0.48	0.38
Wainui-1	Mudstone	0.08	24.21	0.28	0.10	0.28	0.50	12.16	11.52	14.76	73.73	0.46	0.42	0.41
Wainui-1	Mudstone	0.09	28.00	0.27	0.08	0.46	0.29	13.24	15.28	15.83	68.89	0.48	0.47	0.43
Wainui-1	Mudstone	0.13	13.62	0.35	0.08	0.48	0.35	13.19	23.41	16.79	59.80	0.50	0.48	0.44
Wainui-1	Mudstone	0.10	10.00	0.24	0.08	0.35	0.32	10.10	18.40	17.40	64.20	0.47	0.41	0.41
Average		0.10	18.96	0.28	0.08	0.39	0.36	12.17	17.15	16.19	66.65	0.48	0.44	0.42

A: Ts/(Ts + Tm) trisnorhopanes; B: oleanane; C: gammacerane index; D: diahopane/hopane; E: C_{23} tricyclic terpane/(C_{23} tricyclic terpane + C30 hopane); F: C_{19} tricyclic terpane/(C_{23} tricyclic terpane + C_{19} tricyclic terpane); G: steranes/(steranes + hopanes); H: C_{27} steranes; I: C_{28} steranes; J: C_{29} steranes; K: C_{29} diasterane/(C_{29} diasteranes + C_{29} steranes); L: 20s/(20s + 20R) C_{29} Steranes; M: ββ/(αα +ββ) C_{29} steranes.

The coal and mudstone extracts are enriched in C_{29} steranes relative to other steranes (Figure 10B). The extracts are depleted in C_{28} and C_{30} steranes, while diasteranes occur in subordinate contents. Notably, all the extracts are enriched in steranes relative to hopanes with steranes/(steranes + hopanes) average values greater than 5 in all the studied extracts (Table 3). Furthermore, the extracts are enriched in C_{29} steranes relative to C_{27} and C_{28} steranes; however, the coal extracts are more enriched in C_{29} steranes than that in the mudstone extracts (Table 3). In contrast, mudstone extracts are more enriched in diasteranes, thereby displaying an average C_{29} diasteranes/(C_{29} diasteranes + C_{29} steranes) value of 0.48. The coal and mudstone extracts display relatively similar 20s/(20s + 20R) C_{29} steranes and ββ/(αα + ββ) C_{29} steranes values with averages of less than 0.5.

5. Discussion

5.1. Kerogen Compositional Controls on Hydrocarbon Generation

The quantity (TOC content) and quality (kerogen type) of the organic matter in the source rocks determine their ability to generate hydrocarbons [2,3,58]. These factors also control the type and composition of the generated hydrocarbon phases. However, recent studies demonstrated the capability of vitrinite-rich coals to generate liquid hydrocarbon phases even at low levels of oil-window maturity [5,10–12,61]. Geochemical analysis conducted on the studied Rakopi coal and mudstone facies revealed the accumulation of their organofacies in oxic to sub-oxic environments (Figure 4). This is consistent with the elevated pr/ph values in all the studied facies. Such environment did not host favorable conditions for the preservation of organic matter, and thereby bacterial degradation of the organic materials will be more likely. However, the enrichment of the studied facies with organic matter (Figure 5A) is likely attributed to rapid deposition during the peak syn-rift stage, which aided in the preservation of the organic matter (e.g., [8]).

The rapid deposition of the Rakopi facies allowed for the preservation of different maceral facies (Figures 7 and 8). Rakopi coals are enriched in desmocollinite (Figure 7A,C) relative to other vitrinite facies (Figure 7A,C). Several studies demonstrated a good correlation between desmocollinite-rich coals and hydrogen index [62,63], thus typifying the potentiality of these coals to generate liquid hydrocarbon phases. Additionally, several levels within the Rakopi coal seams contain subordinate contents of liptinite and sapropelic organic materials. Specific liptinite facies such as suberinite have excellent capability to generate liquid hydrocarbons (e.g., [64,65]). In addition, suberinite and resinite have greater

potential to generate liquid hydrocarbons even at early stages of oil window maturity (e.g., [66]). Therefore, the presence of desmocollinite, suberinite, and resinite in coal and mudstone facies promote the generation of liquid hydrocarbons despite the overall gas prone kerogen of the Rakopi coals (Figures 5 and 6). The studied coal and mudstone facies are marginally mature (Figure 6B), however, the abundance of suberinite and desmocollinite kerogen likely allowed the generation of liquid hydrocarbon phases even at the early oil window maturity stage.

5.2. Oil–Source Correlation and Implications for Exploration Future in Taranaki Basin

Correlating hydrocarbon phases with their parent source rocks is an essential procedure for hydrocarbon expiration endeavors. A comprehensive oil–source correlation enhances the predictability of hydrocarbon play elements, thereby reduce the exploration risks. The correlation procedure depends on establishing the similarity in specific compositional parameters between the oil and their parent source rocks [3]. These specific parameters include depositional, maturity, and age-relevant biomarkers [3,67–69]. The carbon isotopic composition of saturate and aromatic fractions as well as the deduced canonical variable (CV) values often infer the depositional environment of oils and bitumens. These values effectively differentiate between terrigenous, marine, and mixed depositional environments [70,71]. On the $\delta^{13}C_{saturates}$ versus $\delta^{13}C_{aromatics}$ plot (Figure 11A), coal and mudstone extracts are clustered in the mixed and terrigenous depositional environment, which is consistent with their deposition in a continental to mixed marine environment in agreement with the accumulation of their organic matter in fluvio-deltaic oxygenated conditions (Figure 11B). Notably, oils from nearby discoveries [72] have similar $\delta^{13}C_{saturates}$, $\delta^{13}C_{aromatics}$ values to those observed in the extracts, thus demonstrating a positive oil to extract correlation (Figure 11A,B).

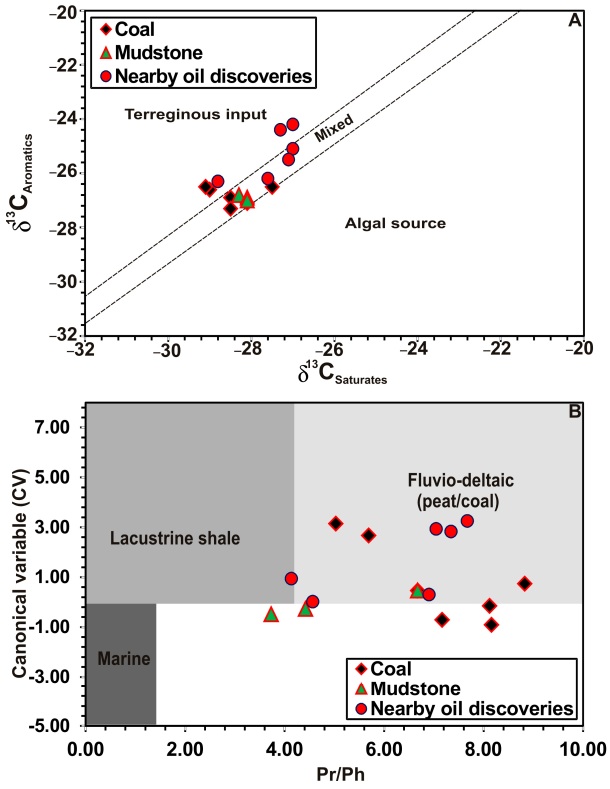

Figure 11. $\delta^{13}C_{saturates}$ versus $\delta^{13}C_{aromatics}$ plot (**A**); the pr/ph versus canonical variable (CV) plot (**B**) illustrate the good correlation between the Rakopi coal, mudstone extracts, and nearby oil discoveries. Interpretation fields are after [70,72].

The isoprenoid (pr, ph) relative to n-alkane (nC_{17}, nC_{18}) values provide insights into the depositional environment and accumulation conditions of the organofacies [3,73]. Both coal and mudstone extracts are dominated by terrigenous input accumulated in sub-oxic conditions in a transitional environment (Figure 12). Most oils from nearby wells have similar isoprenoid ratios to the coal and mudstone extracts, thereby pointing to their positive correlation. Moreover, the relative abundance of C_{27}, C_{28}, and C_{29} steranes is sensitive to the extent of organic input within the kerogen [3,61,74]. Abundance of C_{29} steranes relative to other steranes signifies elevated terrestrial input, whereas abundance of C_{28} steranes is mainly contributes to marine algal input. The coal extracts displaying C_{29} steranes content greater than 70% have a pure terrestrial input, whereas the terrestrial input is relatively lower in the mudstone extracts (Table 3). However, the relative abundance of C_{29} diasteranes in the mudstone extracts confirm their clay-rich content (e.g., [13]). The nearby oil wells display steranes abundance composition revealing their derivation from both the mudstone and coal facies (Figure 13).

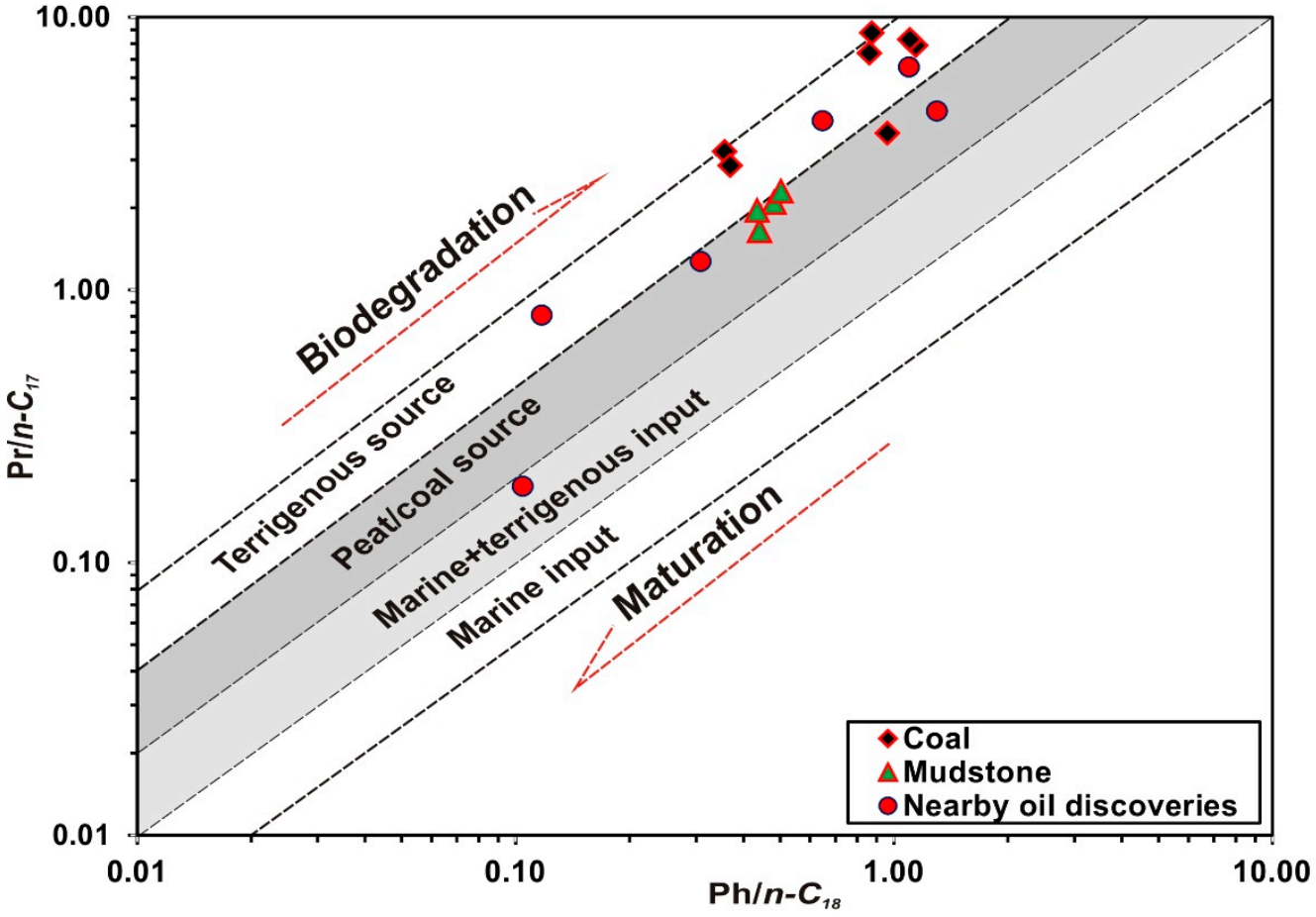

Figure 12. Ph/nC_{18} versus pr/nC_{17} plot demonstrates the terrigenous input in the studied extracts as well as the positive correlation with nearby oil discoveries. Interpretation fields are based on [3].

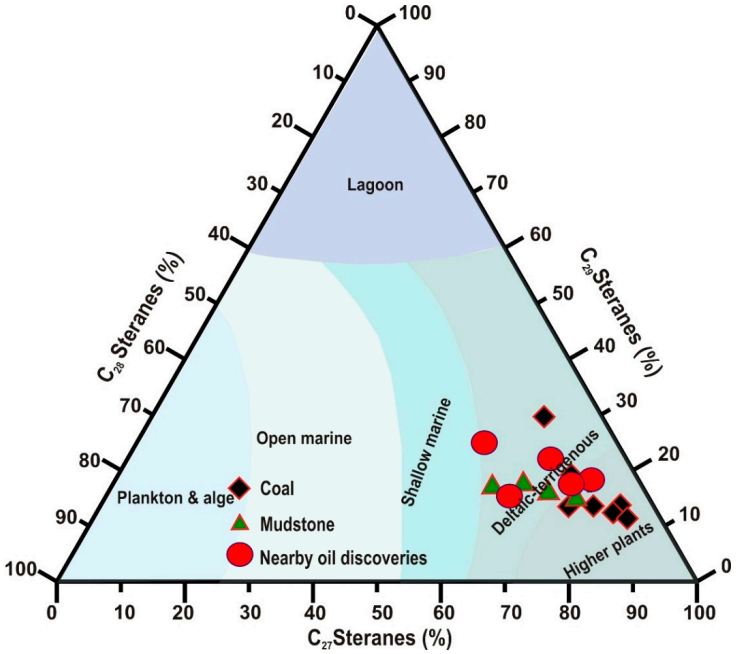

Figure 13. C_{27}, C_{28}, and C_{29} regular steranes plot illustrates the major terrestrial input of the studied extracts and the generation of nearby oils from both coal and mudstone organofacies. Interpretation fields are based on [74].

Maturity-relevant biomarkers such as Ts/(Ts + Tm) trisnorhopanes, 20s/(20s + 20R) C_{29} steranes and ββ/(αα + ββ) C_{29} steranes suggest the marginal to early oil window maturity of the studied coal and mudstone facies (Table 3). Despite the greater vitrinite reflectance values in the mudstone facies (Figure 6B), the relevant biomarkers suggest a similar maturity level for coal and mudstone extracts (Figure 14). Such disturbance in maturity parameters to the early expulsion of the liquid hydrocarbon facies from the mixture desmocollinite-, suberinite-, and resinite-rich kerogen of the coal facies [75]. Therefore, we hypothesize that the onset of hydrocarbon expulsion first started in the coal facies prior to reaching the peak oil window maturity. This is further confirmed by the 20s/(20s + 20R) C_{29} steranes and ββ/(αα + ββ) C_{29} steranes plot, which demonstrates a positive maturity correlation between nearby oil discoveries and the studied extracts (Figure 14).

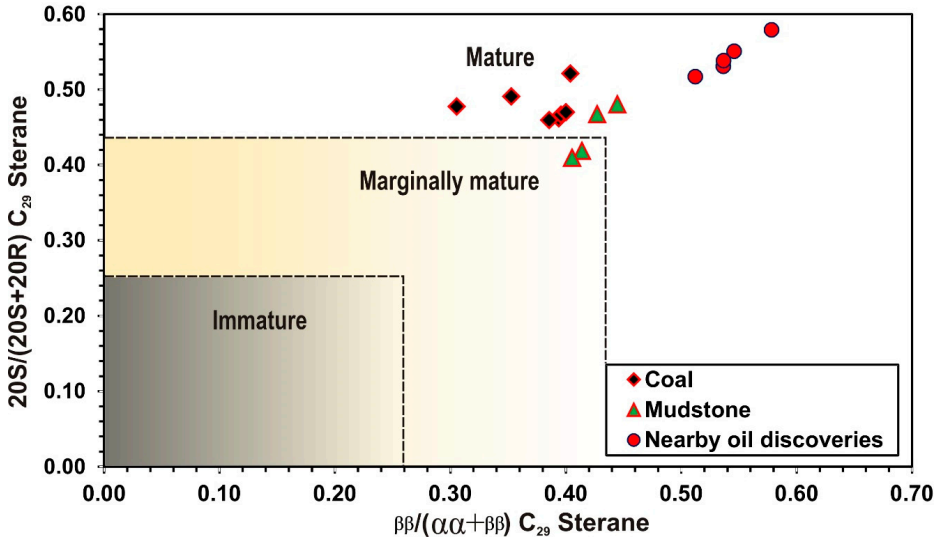

Figure 14. Plot of 20S/(20R + 20S) and ββ/(αα + ββ) C_{29} steranes demonstrates a good maturity correlation between the studied extracts and nearby oil discoveries. Interpretation fields are based on [75].

The positive correlation in depositional-, age-, and maturity-relevant biomarkers between coal, mudstone extracts, and the nearby oil discoveries showed the ability of the Rakopi fluvio-deltaic facies to generate mature liquid hydrocarbon phases. The kerogen composition of the coal facies revealed their ability to generate liquid hydrocarbon at marginal oil window maturity level. At these early maturation levels, light oil is often expelled from coalbeds, in particular those with elevated H/C content, leaving the bitumen behind [76]. Indeed, the compositional attributes in the coal, mudstone extracts, and nearby oils may suggest the contribution of both coal and mudstone facies in oil generation in several parts of the Taranaki Basin. Given the high sorption capacity of the coalbeds [77,78], a greater similarity between expelled oil and remained kerogen in the coal would be expected. However, the sorptive capacity is mostly dependent on the maceral content of coal where greater capacity has been reported in inertinite-rich coals [79]. On the other hand, vitrinite macerals have less sorption capacity. The latter increases in vitrinite-rich coals with increasing the maturity [80]. Considering the marginal oil-window maturity of the studied coal facies along with their vitrinite-rich composition, the retention of the produced oil in the studied coalbeds would be minimal.

6. Conclusions

- The upper Cretaceous coal and mudstone facies of the Rakopi Formation host potential organofacies in the Taranaki Basin, New Zealand. These lithofacies have high TOC (average > 20 wt%) despite their deposition in oxygenated bottom water conditions (TOC/TS > 5).
- Rakopi coals are enriched in desmocollinite, suberinite, and resinite macerals, whereas the mudstone facies are enriched in liptodetrinite and cutinite. Vitrinite reflectance is greater in mudstone than that in coal lithofacies.
- Extracts from the coal and mudstone lithofacies have similar compositional attributes, however, the coal extracts have greater input from terrestrial materials.
- Maturity-relevant biomarkers elucidate similar levels of maturity, suggesting an early phase of expulsion from the coal lithofacies.
- Correlation between compositional markers in coal, mudstone extracts, and nearby oil discoveries revealed a mixing signature between oil derived from coal and mudstone organofacies, despite the variable levels of maturity.
- The present results demonstrate the ability of marginal mature coals to generate liquid hydrocarbon phases, thereby opening new frontiers for exploration in several regions of the Taranaki Basin.

Author Contributions: M.L.: Conceptualization, Methodology, Software, Validation, Writing—Original Draft Preparation, Visualization. A.A.R.: Writing—review and editing, Methodology, Interpretation, Software, Visualization. M.I.A.-F.: Writing—review and editing, Methodology, Visualization. All authors have read and agreed to the published version of the manuscript.

Funding: This research received no external funding.

Data Availability Statement: The raw materials utilized in this work will be made available upon request from the corresponding author.

Acknowledgments: The authors express their gratitude to the New Zealand Petroleum & Minerals Authority and the GNS Science of New Zealand for releasing the data and provide the necessary permission for dissemination and publication of the present results.

Conflicts of Interest: The authors declare no conflict of interest.

References

1. Hunt, M.J. Organic geochemistry of the marine environment. In *Advances in Organic Geochemistry*; Tissot, B., Bienner, F., Eds.; Pergamon Press: Oxford, UK, 1974; pp. 597–605.
2. Peters, K.E.; Cassa, M.R. Applied source rock geochemistry. In *The Petroleum System from Source to Trap*; Magoon, L.B., Dow, W.G., Eds.; AAPG: Tulsa, OK, USA, 1994; pp. 93–117.

3. Peters, E.K.; Walters, C.C.; Moldowan, M.J. The Biomarker guide. In *Biomarkers and Isotopes in the Environment and Human History*, 2nd ed.; Cambridge University Press: Cambridge, UK, 2005; Volume I, p. 471.
4. El Matboly, E.; Leila, M.; Peters, K.; El Diasty, W. Oil biomarker signature and hydrocarbon prospectivity of paleozoic versus mesozoic source rocks in the Faghur–Sallum basins, Egypt's Western Desert. *J. Pet. Sci. Eng.* **2022**, *217*, 110872. [CrossRef]
5. Mahmoud, A.I.; Metwally, A.M.; Mabrouk, W.M.; Leila, M. Controls on hydrocarbon accumulation in the pre-rift paleozoic and late syn-rift cretaceous sandstones in PTAH oil field, north Western Desert, Egypt: Insights from seismic stratigraphy, petrophysical rock-typing and organic geochemistry. *Mar. Pet. Geol.* **2023**, *155*, 106398. [CrossRef]
6. Pedersen, T.; Calvert, S.E. Anoxia vs. productivity: What controls the formation of organic-carbon-rich sediments and sedimentary rocks? *AAPG Bull.* **1990**, *74*, 454–466.
7. Akande, S.O.; Egenhoff, S.O.; Obaje, N.G.; Ojo, O.J.; Adekeye, O.A.; Erdtmann, B.D. Hydrocarbon potential of Cretaceous sediments in the Lower and Middle Benue Trough, Nigeria: Insights from new source rock facies evaluation. *J. Afr. Earth Sci.* **2012**, *64*, 34–47. [CrossRef]
8. Fathy, D.; Abart, R.; Wagreich, M.; Gier, S.; Ahmed, M.S.; Sami, M. Late Campanian Climatic-Continental Weathering Assessment and Its Influence on Source Rocks Deposition in Southern Tethys, Egypt. *Minerals* **2023**, *13*, 160. [CrossRef]
9. Lewan, M.D.; Ruble, T.E. Comparison of petroleum generation kinetics by isothermal hydrous and nonisothermal open-system pyrolysis. *Org. Geochem.* **2002**, *33*, 1457–1475. [CrossRef]
10. Leila, M.; Loiseau, K.; Moretti, I. Controls on generation and accumulation of blended gases (CH4/H2/He) in the Neoproterozoic Amadeus Basin, Australia. *Marine and Petroleum Geology* **2022**, *140*, 105643. [CrossRef]
11. Leila, M.; Awadalla, A.; Farag, A.; Moscariello, A. Organic geochemistry and oil-source rock correlation of the Cretaceous succession in West Wadi El-Rayan (WWER) concession: Implications for a new Cretaceous petroleum system in the north Western Desert, Egypt. *J. Pet. Sci. Eng.* **2022**, *219*, 111071. [CrossRef]
12. Stockhausen, M.; Galimberti, R.; Elias, R.; Di Paolo, L.; Schwark, L. Expulsinator assessment of oil/ gas generation and expulsion characteristics of different source rocks. *Mar. Pet. Geol.* **2021**, *129*, 105057. [CrossRef]
13. Weston, R.J.; Engel, M.H.; Philp, R.P.; Woolhouse, A.D. The stable carbon isotopic composition of oil from the Taranaki Basin of New Zealand. *Org. Geochem.* **1988**, *12*, 487–493. [CrossRef]
14. Johnston, J.; Collier, R.; Maidment, A. Coals as source rocks for hydrocarbon generation in the Taranaki Basin, New Zealand: A geochemical biomarker study. *J. Southeast Asian Earth Sci.* **1991**, *5*, 283–289. [CrossRef]
15. King, P.R.; Thrasher, G.P. *Cretaceous-Cenozoic Geology and Petroleum Systems of the Taranaki Basin, New Zealand*; Institute of Geological & Nuclear Sciences Monograph: Lower Hutt, New Zealand, 1996; Volume 13, p. 244.
16. Higgs, K.; King, P.; Raine, J.; Sykes, R.; Browne, G.; Crouch, E.; Baur, J. Sequence stratigraphy and controls on reservoir sandstone distribution in an Eocene marginal marine-coastal plain fairway, Taranaki Basin, New Zealand. *Mar. Pet. Geol.* **2012**, *32*, 110–137. [CrossRef]
17. Higgs, K.; Crouch, E.; Raine, J. An interdisciplinary approach to reservoir characterisation; an example from the early to middle Eocene Kaimiro Formation, Taranaki Basin, New Zealand. *Mar. Pet. Geol.* **2017**, *86*, 111–139. [CrossRef]
18. Kumar, P.C.; Sain, K. Attribute amalgamation-aiding interpretation of faults from seismic data: An example from Waitara 3D prospect in Taranaki basin off New Zealand. *J. Appl. Geophys.* **2018**, *159*, 52–68. [CrossRef]
19. Leila, M.; El-Sheikh, I.; Abdelmaksoud, A.; Radwan, A.A. Seismic sequence stratigraphy and depositional evolution of the Cretaceous-Paleogene sedimentary successions in the offshore Taranaki Basin, New Zealand: Implications for hydrocarbon exploration. *Mar. Geophys. Res.* **2022**, *43*, 23. [CrossRef]
20. Abdelmaksoud, A.; Radwan, A.A. Integrating 3D seismic interpretation, well log analysis and static modelling for characterizing the Late Miocene reservoir, Ngatoro area, New Zealand. *Géoméch. Geophys. Geo-Energy Geo-Resour.* **2022**, *8*, 63. [CrossRef]
21. Radwan, A.A.; Nabawy, B.S.; Shihata, M.; Leila, M. Seismic interpretation, reservoir characterization, gas origin and entrapment of the Miocene-Pliocene Mangaa C sandstone, Karewa Gas Field, North Taranaki Basin, New Zealand. *Mar. Pet. Geol.* **2021**, *135*, 105420. [CrossRef]
22. Katz, H.R. Potential oil formations in New Zealand, and their stratigraphic position as related to basin evolution. *New Zealand J. Geol. Geophys.* **1968**, *11*, 1077–1133. [CrossRef]
23. Czochanska, Z.; Gilbert, T.; Philp, R.; Sheppard, C.; Weston, R.; Wood, T.; Woolhouse, A. Geochemical application of sterane and triterpane biomarkers to a description of oils from the Taranaki Basin in New Zealand. *Org. Geochem.* **1988**, *12*, 123–135. [CrossRef]
24. Collier, R.; Johnston, J. The identification of possible hydrocarbon source rocks, using biomarker geochemistry, in the Taranaki basin, New Zealand. *J. Southeast Asian Earth Sci.* **1991**, *5*, 231–239. [CrossRef]
25. Killops, S.; Frewin, N. Triterpenoid diagenesis and cuticular preservation. *Org. Geochem.* **1994**, *21*, 1193–1209. [CrossRef]
26. Murray, A.P.; Summons, R.E.; Boreham, C.J.; Dowling, L.M. Biomarker and n-alkane isotope profiles for Tertiary oils: Relationship to source rock depositional setting. *Org. Geochem.* **1994**, *22*, 521–542, IN5–IN6. [CrossRef]
27. Killops, S.; Raine, J.; Woolhouse, A.; Weston, R. Chemostratigraphic evidence of higher-plant evolution in the Taranaki Basin, New Zealand. *Org. Geochem.* **1995**, *23*, 429–445. [CrossRef]
28. Killops, S.; Funnell, R.; Suggate, R.; Sykes, R.; Peters, K.; Walters, C.; Woolhouse, A.; Weston, R.; Boudou, J.-P. Predicting generation and expulsion of paraffinic oil from vitrinite-rich coals. *Org. Geochem.* **1998**, *29*, 1–21. [CrossRef]
29. Sykes, R.; Snowdon, L. Guidelines for assessing the petroleum potential of coaly source rocks using Rock-Eval pyrolysis. *Org. Geochem.* **2002**, *33*, 1441–1455. [CrossRef]

30. Wilkins, R.W.; George, S.C. Coal as a source rock for oil: A review. *Int. J. Coal Geol.* **2002**, *50*, 317–361. [CrossRef]
31. Sykes, R.; Volk, H.; George, S.; Ahmed, M.; Higgs, K.; Johansen, P.; Snowdon, L. Marine influence helps preserve the oil potential of coaly source rocks: Eocene Mangahewa Formation, Taranaki Basin, New Zealand. *Org. Geochem.* **2014**, *66*, 140–163. [CrossRef]
32. Qadri, S.M.T.; Shalaby, M.; Islam, A.; Hoon, L.L. Source rock characterization and hydrocarbon generation modeling of the Middle to Late Eocene Mangahewa Formation in Taranaki Basin, New Zealand. *Arab. J. Geosci.* **2016**, *9*, 559. [CrossRef]
33. Makeen, Y.M.; Abdullah, W.H.; Hakimi, M.H.; Mustapha, K.A. Source rock characteristics of the Lower Cretaceous Abu Gabra Formation in the Muglad Basin, Sudan, and its relevance to oil generation studies. *Mar. Pet. Geol.* **2015**, *59*, 505–516. [CrossRef]
34. El-Shafeiy, M.; El-Kammar, A.; El-Barkooky, A.; Meyers, P.A. Paleo-redox depositional conditions inferred from trace metal accumulation in two Cretaceous-Paleocene organic-rich sequences from Central Egypt. *Mar. Pet. Geol.* **2016**, *73*, 333–349. [CrossRef]
35. Cao, J.; Yang, R.; Yin, W.; Hu, G.; Bian, L.; Fu, X. Mechanism of Organic Matter Accumulation in Residual Bay Environments: The Early Cretaceous Qiangtang Basin, Tibet. *Energy Fuels* **2018**, *32*, 1024–1037. [CrossRef]
36. Palmer, J.A.; Andrews, P.B. Cretaceous–Tertiary sedimentation and implied tectonic controls on the structural evolution of Taranaki Basin, New Zealand. South Pacific sedimentary basins. *Sediment. Basins World* **1993**, *2*, 309–328.
37. Sutherland, R.; King, P.; Wood, R. Tectonic evolution of Cretaceous rift basins in southeastern Australia and New Zealand: Implications for exploration risk assessment. In *Eastern Australasian Basins Symposium*; Hill, K.C., Bernecker, T., Eds.; Petroleum Exploration Society of Australia Special Publication; Petroleum Exploration Society of Australia: Perth, Australia, 2001; pp. 3–13.
38. Sutherland, R.; Collot, J.; Lafoy, Y.; Logan, G.A.; Hackney, R.; Stagpoole, V.; Uruski, C.; Hashimoto, T.; Higgins, K.; Herzer, R.H.; et al. Lithosphere delamination with foundering of lower crust and mantle caused permanent subsidence of New Caledonia Trough and transient uplift of Lord Howe Rise during Eocene and Oligocene initiation of Tonga-Kermadec subduction, western Pacific. *Tectonics* **2010**, *29*, TC2004. [CrossRef]
39. Kumar, P.C.; Omosanya, K.O.; Eruteya, O.E.; Sain, K. Geomorphological characterization of basal flow markers during recurrent mass movement: A case study from the Taranaki Basin, offshore New Zealand. *Basin Res.* **2021**, *33*, 2358–2382. [CrossRef]
40. Radwan, A.A.; Nabawy, B.S.; Abdelmaksoud, A.; Lashin, A. Integrated sedimentological and petrophysical characterization for clastic reservoirs: A case study from New Zealand. *J. Nat. Gas Sci. Eng.* **2021**, *88*, 103797. [CrossRef]
41. Radwan, A.A.; Nabawy, B.S. Hydrocarbon prospectivity of the miocene-pliocene clastic reservoirs, Northern Taranaki basin, New Zealand: Integration of petrographic and geophysical studies. *J. Pet. Explor. Prod. Technol.* **2022**, *12*, 1945–1962. [CrossRef]
42. Elmahdy, M.; Radwan, A.A.; Nabawy, B.S.; Abdelmaksoud, A.; Nastavkin, A.V. Integrated geophysical, petrophysical and petrographical characterization of the carbonate and clastic reservoirs of the Waihapa Field, Taranaki Basin, New Zealand. *Mar. Pet. Geol.* **2023**, *151*, 106173. [CrossRef]
43. Radwan, A.A.; Nabawy, B.S.; Kassem, A.A.; Elmahdy, M. An integrated workflow for seismic interpretation, petrophysical and petrographical characterization for the clastic Mangahewa reservoir in Pohokura gas field, Taranaki Basin, New Zealand. *Geoenergy Sci. Eng.* **2023**, *229*, 212117. [CrossRef]
44. Shalaby, M.R.; Malik, O.A.; Lai, D.; Jumat, N.; Islam, M.A. Thermal maturity and TOC prediction using machine learning techniques: Case study from the Cretaceous–Paleocene source rock, Taranaki Basin, New Zealand. *J. Pet. Explor. Prod. Technol.* **2020**, *10*, 2175–2193. [CrossRef]
45. Schellart, W.; Lister, G.; Toy, V. A Late Cretaceous and Cenozoic reconstruction of the Southwest Pacific region: Tectonics controlled by subduction and slab rollback processes. *Earth-Sci. Rev.* **2006**, *76*, 191–233. [CrossRef]
46. Strogen, D.P.; Bland, K.J.; Nicol, A.; King, P.R. Paleogeography of the Taranaki Basin region during the latest Eocene–Early Miocene and implications for the 'total drowning'of Zealandia. *N. Zealand J. Geol. Geophys.* **2014**, *57*, 110–127. [CrossRef]
47. Grahame, J. Deepwater Taranaki Basin, New Zealand—New interpretation and modelling results for Large Scale Neogene Channel and Fan Systems: Implications for hydrocarbon prospectivity. In Proceedings of the AAPG/SEG 2015 International Conference and Exhibition (ICE), A Powerhouse Emerges: Energy for the Next Fifty Years, Melbourne, Australia, 13–16 September 2015.
48. Behar, F.; Beaumont, V.D.E.B.; Penteado, H.D.B. Rock-Eval 6 Technology: Performances and Developments. *Oil Gas Sci. Technol.* **2001**, *56*, 111–134. [CrossRef]
49. Wu, M.; Shen, J.; Qin, Y.; Qin, Y.; Wang, X.; Zhu, S. Method of Identifying Total Sulfur Content in Coal: Geochemical and Geophysical Logging Data from the Upper Paleozoic in North China. *ACS Omega* **2022**, *7*, 45045–45056. [CrossRef] [PubMed]
50. Mukhopadhyay, P.K. Maturation of organic matter as revealed by microscopic methods: Applications and limitations of vitrinite reflectance, and continuous spectral and pulsed laser fluorescence spectroscopy. In *Developments in Sedimentology*; Elsevier: Amsterdam, The Netherlands, 1992; Volume 47, pp. 435–510.
51. Rogers, K.M.; Collen, J.D.; Johnston, J.H.; Elgar, N.E. A geochemical appraisal of oil seeps from the East Coast Basin, New Zealand. *Org. Geochem.* **1999**, *30*, 593–605. [CrossRef]
52. A Berner, R.; Raiswell, R. Burial of organic carbon and pyrite sulfur in sediments over phanerozoic time: A new theory. *Geochim. Et Cosmochim. Acta* **1983**, *47*, 855–862. [CrossRef]
53. Hedges, J.I.; Keil, R.G. Sedimentary organic matter preservation: An assessment and speculative synthesis. *Mar. Chem.* **1995**, *49*, 81–115. [CrossRef]
54. Fathy, D.; Wagreich, M.; Fathi, E.; Ahmed, M.S.; Leila, M.; Sami, M. Maastrichtian Anoxia and Its Influence on Organic Matter and Trace Metal Patterns in the Southern Tethys Realm of Egypt during Greenhouse Variability. *ACS Omega* **2023**, *8*, 19603–19612. [CrossRef] [PubMed]

55. Cornford, C.; Rullkotter, J.; Welte, D. Organic geochemistry of DSDP Leg 47a, Site 397, eastern North Atlantic: Organic petrography and extractable hydrocarbons. *Initial Rep. Deep Sea Drill. Proj.* **1979**, *47 Pt 1*, 511–522.
56. Dutta, S.; Mathews, R.P.; Singh, B.D.; Tripathi, S.M.; Singh, A.; Saraswati, P.K.; Banerjee, S.; Mann, U. Petrology, palynology and organic geochemistry of Eocene lignite of Matanomadh, Kutch Basin, western India: Implications to depositional environment and hydrocarbon source potential. *Int. J. Coal Geol.* **2011**, *85*, 91–102. [CrossRef]
57. Tao, S.; Wang, Y.; Tang, D.; Wu, D.; Xu, H.; He, W. Organic petrology of Fukang Permian Lucaogou Formation oil shales at the northern foot of Bogda Mountain, Junggar Basin, China. *Int. J. Coal Geol.* **2012**, *99*, 27–34. [CrossRef]
58. Tissot, B.P.; Welte, D.H. Kerogen: Composition and Classification. In *Petroleum Formation and Occurrence*; Springer: Berlin/Heidelberg, Germany, 1984; pp. 131–159.
59. Mello, M.; Gaglianone, P.; Brassell, S.; Maxwell, J. Geochemical and biological marker assessment of depositional environments using Brazilian offshore oils. *Mar. Pet. Geol.* **1988**, *5*, 205–223. [CrossRef]
60. Peters, K.E.; Fraser, T.H.; Amris, W.; Rustanto, B.; Hermanto, E. Geochemistry of crude oils from eastern Indonesia. *AAPG Bull.* **1999**, *83*, 1927–1942.
61. Hassan, M.; Leila, M.; Ahmed, M.; Issa, G.; Hegab, O. Geochemical characteristics of natural gases and source rocks in Obayied sub-basin, north Western Desert, Egypt: Implications for gas-source correlation. *Acta Geochim.* **2023**, *42*, 241–255. [CrossRef]
62. Zhao, C.Y.; Cheng, K.M. The Organic Petrology Characteristics of Oil Derived from Coal in Turpan-Hami Basin. *Pet. Explor. Dev.* **1995**, *22*, 24–27.
63. Li, C.; Yuan, Q.; Zhang, M. Generative Potential of Carboniferous-Permian Coal-Bearing Source Rocks in Ordos Basin. *Open J. Yangtze Oil Gas* **2021**, *2*, 260–272. [CrossRef]
64. Wan Hasiah, A. Evidence of early generation of liquid hydrocarbon from suberinite as visible under the microscope. *Org. Geochem.* **1997**, *27*, 591–596. [CrossRef]
65. Yao, S.; Cao, J.; Zhang, K.; Jiao, K.; Ding, H.; Hu, W. Artificial bacterial degradation and hydrous pyrolysis of suberin: Implications for hydrocarbon generation of suberinite. *Org. Geochem.* **2012**, *47*, 22–33. [CrossRef]
66. Pickel, W.; Kus, J.; Flores, D.; Kalaitzidis, S.; Christanis, K.; Cardott, B.J.; Misz-Kennan, M.; Rodrigues, S.; Hentschel, A.; Hamor-Vido, M.; et al. Classification of liptinite–ICCP System 1994. *Int. J. Coal Geol.* **2017**, *169*, 40–61. [CrossRef]
67. Waples, D.W. Source-Rock Evaluation. In *Geochemistry in Petroleum Exploration*; Springer: Berlin/Heidelberg, Germany, 1985; pp. 93–120.
68. Magoon, L.B.; Dow, W.G. The Petroleum System. In *The Petroleum System—From Source to Trap*; Magoon, L.B., Dow, W.G., Eds.; AAPG Memoire; AAPG: Tulsa, OK, USA, 1994; Volume 60, pp. 3–24.
69. Dembicki, H., Jr. *Practical Petroleum Geochemistry for Exploration and Production*; Elsevier: Amsterdam, The Netherlands, 2017; p. 331.
70. Sofer, Z. Stable Carbon Isotope Compositions of Crude Oils: Application to Source Depositional Environments and Petroleum Alteration. *AAPG Bull.* **1984**, *68*, 31–49.
71. Peters, K.; Moldowan, J. Effects of source, thermal maturity, and biodegradation on the distribution and isomerization of homohopanes in petroleum. *Org. Geochem.* **1991**, *17*, 47–61. [CrossRef]
72. Sykes, R. Chemometric Classification of Terrestrial Oil Families in Taranaki Basin, New Zealand: Higher Plant Trends and Migration Contamination Effects. In Proceedings of the AAPG Hedberg Conference, The Evolution of Petroleum Systems Analysis: Changing of the Guard from Late Mature Experts to Peak Generating Staff, Houston, TX, USA, 4–6 March 2019.
73. Shanmugam, G. Significance of Coniferous Rain Forests and Related Organic Matter in Generating Commercial Quantities of Oil, Gippsland Basin, Australia. *AAPG Bull.* **1985**, *69*, 1241–1254. [CrossRef]
74. Huang, W.Y.; Meinschein, W.G. Sterols as ecological indicators. *Geochim. Et Cosmochim. Acta* **1979**, *43*, 739–745. [CrossRef]
75. Seifert, W.K.; Moldowan, J.M. Use of biological markers in petroleum exploration. *Methods Geochem. Geophys.* **1986**, *24*, 261–290.
76. Glikson, M.; Boreham, C.; Thiede, D. Coal composition and mode of maturation, a determination factor in quantifying hydrocarbon species generated. In *Coalbed Methane: Scientific, Environmental and Economic Evaluation*; Mastalerz, M., Glikson, M., Golding, S., Eds.; Springer: Berlin/Heidelberg, Germany, 1999; pp. 155–158.
77. Cooles, G.; Mackenzie, A.; Quigley, T. Calculation of petroleum masses generated and expelled from source rocks. *Org. Geochem.* **1986**, *10*, 235–245. [CrossRef]
78. Sandvik, E.; Young, W.; Curry, D. Expulsion from hydrocarbon sources: The role of organic absorption. *Org. Geochem.* **1992**, *19*, 7–87. [CrossRef]
79. Stach, E.; Mackowsky M-Th Teichmuller, M.; Taylor, G.H.; Chandra, D.; Teichmuller, R. *Stach's Textbook of Coal Petrology*, 3rd ed.; Gebruder Borntraeger: Stuttgart, Germany, 1982; 535p.
80. Levine, J.R. Coalification: The evolution of coal as source rock and reservoir rock for oil and gas. In *Hydrocarbons from Coal: AAPG Studies in Geology #38*; Law, B.E., Rice, D.D., Eds.; AAPG: Tulsa, OK, USA, 1993; pp. 39–77.